Soret coefficient for liquid argon-krypton mixtures via equilibrium and nonequilibrium molecular dynamics: A comparison with experiments

A. Perronace,[1,*] G. Ciccotti,[2] F. Leroy,[1] A. H. Fuchs,[1] and B. Rousseau[1]
[1]*Laboratoire de Chimie-Physique, Bâtiment 350, Université de Paris-Sud, 91405 Orsay, France*
[2]*INFM and Dipartimento di Fisica, Università degli Studi di Roma "La Sapienza," Piazzale Aldo Moro 2, I-00185 Roma, Italy*
(Received 4 February 2002; revised manuscript received 10 May 2002; published 18 September 2002)

The Soret and the other transport coefficients, characterizing the heat and mass transport in binary mixtures, have been obtained by equilibrium and nonequilibrium molecular dynamics (EMD and NEMD, respectively). Two state points of the argon-krypton mixture are considered, for which experimental values of the Soret coefficient are available. To attempt a comparison between simulations and experiments the common enthalpy-diffusion-free expression for the heat flux has been chosen. The comparison of the simulations with the experiments shows a remarkable agreement, for all the several utilized EMD and NEMD techniques (dynamical and stationary). The techniques, used over 0.3 μs of total simulation time span, are slow convergent but have comparable performances.

DOI: 10.1103/PhysRevE.66.031201 PACS number(s): 66.10.Cb

I. INTRODUCTION

In a binary isotropic mixture thermal and diffusive transport properties are described by four phenomenological coefficients in the absence of chemical reactions and external forces, for other effects do not couple with thermal phenomena (Curie's principle). Two of them govern direct transport—i.e., particle flow induced by a concentration gradient and heat flow caused by a thermal gradient—as in one-component fluids. The other two are connected to the cross coupling of diffusive and thermal flows. These two coefficients are equal in the linear regime [as stated by the so-called Onsager's reciprocity relations (ORR)]—i.e., for weak thermal and chemical potential gradients. In this work we are particularly concerned with these cross coefficients, which are generally difficult to obtain with a good accuracy, since they are rather small compared to the direct ones.

The phenomenological coefficients for a Lennard-Jones Ar-Kr liquid mixture, equimolar and close to the triple point, were first calculated by MacGowan and Evans (ME) [1], and then confirmed by Paolini and Ciccotti (PC) [2]. In Ref. [1], ME, equilibrium and nonequilibrium molecular dynamics (respectively, EMD and NEMD) were performed using an approximate microscopic expression for the heat flux and looking at the stationary response of the system. In Ref. [2], PC, the same methods were applied, but looking at the dynamical (transient-time) response of the system, with the help, for small applied fields, of a noise reduction technique (substraction technique). It was also pointed out that the approximation for the heat flux corresponds to assume as ideal the mixture, i.e., the interaction between is identical to that within components [3]. In a subsequent paper, Vogelsang *et al.* [4] used both the NEMD data of PC and ME for comparing with longer EMD simulations that made use of the rigorous expression for the microscopic heat flux. More specifically, they reconstructed the exact expression of the heat flux by plugging in the rigourous partial enthalpies of the mixture instead of the approximate instantaneous values of ME. As a result of this study, the approximate and correct heat flux expressions gave consistent values for the phenomenological coefficients.

The four phenomenological coefficients can be used, in conjunction with thermodynamic quantities such as partial enthalpies and chemical potential derivatives, to calculate thermal conductivity, Soret, thermal diffusion, and mutual diffusion coefficients. These are the transport coefficients usually measured in experiments. In this work, the theoretical relation between the directly simulated quantities and the experimental coefficients has been reviewed.

We performed EMD and NEMD (dynamical and stationary) calculations of the Soret and the other thermal diffusion coefficients for two Ar-Kr state points. These mixtures were experimentally studied by Longrée *et al.* [5,6], and are rather far away from the triple point studied by ME and PC. The above ideal mixture approximation has been used.

The plan of the paper is as follows. In Sec. II we specify the formalism we use. We give the relations between phenomenological and experimental transport coefficients and introduce the general formalism for the response theory followed by a description of several measurement techniques. In Sec. III we present the model chosen for the mixtures and the states studied. In Sec. IV, we present and discuss the simulation results for the transport coefficients. We compare the validity and efficiency of the different techniques and study the ORR out of the linear regime. Finally, conclusions are drawn in Sec. V.

II. FORMALISM

A. Phenomenological equations

The macroscopic relations describing the transport of matter and heat in a two-component isotropic mixture can be expressed, in the framework of irreversible thermodynamics, as [7]

*Present address: Ing. Barzano' & Zanardo S.p.A., via Piemonte 26, I-00187 Roma, Italy.

$$\mathbf{J}_E = -\tilde{L}_{EE}\frac{\nabla T}{T^2} - \sum_{\beta=1}^{2} \tilde{L}_{E\beta}\nabla\left(\frac{\mu_\beta}{T}\right), \tag{1a}$$

$$\mathbf{J}_\alpha = -\tilde{L}_{\alpha E}\frac{\nabla T}{T^2} - \sum_{\beta=1}^{2} \tilde{L}_{\alpha\beta}\nabla\left(\frac{\mu_\beta}{T}\right), \tag{1b}$$

where $\mathbf{J}_\alpha$ is the mass flux of species α relative to the center-of-mass frame (for a binary mixture we have $\mathbf{J}_2 = -\mathbf{J}_1$), $\mathbf{J}_E$ is the energy flow excluding convection, μ_β is the chemical potential of species β, T is the temperature, and the $\tilde{L}_{\alpha\beta}$'s are the phenomenological coefficients of energy and particle transport in a mixture. Since we have used, for the thermodynamic forces, the expressions appearing in the entropy production term, the Onsager equality holds for the cross coefficients, i.e., $\tilde{L}_{E\beta} = \tilde{L}_{\beta E}$ [7]. Equations (1) are written using the Curie's principle, i.e., generalized forces of different tensorial character do not couple in isotropic mixtures. To calculate the experimentally defined transport coefficients, we have to compare the phenomenological Eqs. (1) with the constitutive equations used by experimentalists [8],

$$\mathbf{J}_Q = -\lambda\nabla T - \rho w_1 \mu_{11}^w T D_T^D \nabla w_1, \tag{2a}$$

$$\mathbf{J}_1 = -\rho w_1 w_2 D_T \nabla T - \rho D \nabla w_1, \tag{2b}$$

with λ the thermal conductivity, D the mutual diffusion, D_T the thermal diffusion, and D_T^D the Dufour coefficients; the quantity w_α is the mass fraction of species α and μ_{11}^w the derivative of the chemical potential of species 1 with respects to w_1. The mass flux $\mathbf{J}_1$ is measured in the center-of-mass reference.

In Eqs. (2) we have the *heat flux* $\mathbf{J}_Q$, while in Eqs. (1) we have the *energy flux* $\mathbf{J}_E$. We therefore have to cast the relations (1) in a form suitable for the comparison, that is we have to pass from $\mathbf{J}_E$ to $\mathbf{J}_Q$. Several definitions of $\mathbf{J}_Q$ have been proposed [9] since a clear physical definition of it in mixtures is lacking. Therefore, a certain arbitrariness in the choice remains. One of the most used is [1,2,4]

$$\mathbf{J}_Q = \mathbf{J}_E - \sum_\alpha \frac{h_\alpha}{m_\alpha}\mathbf{J}_\alpha, \tag{3}$$

with m_α the mass of a particle of component α, h_α the partial enthalpy of component α, that is $h_\alpha = (\partial H/\partial N_\alpha)_{P,T,\{N_\beta\}}$ with $\{N_\beta\}$ the set of particle numbers of all the components but the α. In the present paper we *assume* $\mathbf{J}_E$ to be the correct choice for the heat flux measured in experiments.

Inserting Eq. (3) into Eqs. (1), expressing the chemical potential gradients as functions of concentrations, and carrying out the algebra, we end up with the phenomenological equations which include the gradients measured in experiments,

$$\mathbf{J}_Q = -L_{QQ}\frac{\nabla T}{T^2} - L_{Q1}\frac{\mu_{11}^w}{w_2 T}\nabla w_1, \tag{4a}$$

$$\mathbf{J}_1 = -L_{1Q}\frac{\nabla T}{T^2} - L_{11}\frac{\mu_{11}^w}{w_2 T}\nabla w_1. \tag{4b}$$

We can now compare Eqs. (4) to the Eqs. (2) and make the identification [7]

$$\lambda = \frac{L_{QQ}}{T^2}, \tag{5a}$$

$$D = \frac{L_{11}\mu_{11}^w}{\rho w_2 T}, \tag{5b}$$

$$D_T^D = \frac{L_{Q1}}{\rho w_1 w_2 T^2}, \quad D_T = \frac{L_{1Q}}{\rho w_1 w_2 T^2}, \tag{5c}$$

$$\frac{D_T}{D} \equiv S_T = \frac{L_{Q1}}{L_{11}\mu_{11}^w T w_1}. \tag{5d}$$

The coefficients $L_{\alpha\beta}$'s can be written as functions of the $\tilde{L}_{\alpha\beta}$'s and the h_α's. Hence, the transport coefficients (5) can be expressed in terms of the $\tilde{L}_{\alpha\beta}$'s. This could be of some interest for the simulation, since $\mathbf{J}_Q$ does not have a fully microscopic expression (it is not a full phase function since it contains thermodynamic quantities), while $\mathbf{J}_E$ does. The only exception is for mixtures with equal intermolecular potentials for each component, i.e., isotopic. In this case one can give a microscopic expression for the heat flux (see the following section) which is found valid also for the more general case of ideal mixtures [4], i.e., with mixtures with negligible excess quantities. Therefore, in the ideal case, we need not calculate, by independent simulations, the partial enthalpies. Moreover, in this case, we have an analytical expression for μ_{11}^w [7],

$$\mu_{11}^w = \frac{RT}{w_1[M_1 - w_1(M_1 - M_2)]}, \tag{6}$$

with R the gas constant. Thus, by using Eq. (6) and calculating the $L_{\alpha\beta}$'s directly in a simulation of an ideal mixture, we obtain the transport coefficients (5).

B. Microscopic fluxes

We consider a system of N particles, N_1 of mass m_1 and N_2 of mass m_2, with coordinates $\mathbf{r}_{i\alpha}$ and momenta $\mathbf{p}_{i\alpha}$, where $\alpha = 1,2$ runs over different species, $i = 1,2,\ldots,N_\alpha$ over all particles belonging to species α. Let $\mathbf{r}_{i\alpha,j\beta}$ be the relative position of the particles $i\alpha$ and $j\beta$, $e_{i\alpha}$ the total energy of particle $i\alpha$, and $\mathbf{F}_{i\alpha,j\beta}$ the force on $i\alpha$ due to $j\beta$,

$$\mathbf{r}_{i\alpha,j\beta} = \mathbf{r}_{i\alpha} - \mathbf{r}_{j\beta}, \quad r_{i\alpha,j\beta} = |\mathbf{r}_{i\alpha} - \mathbf{r}_{j\beta}|, \tag{7a}$$

$$e_{i\alpha} = \frac{|\mathbf{p}_{i\alpha}|^2}{2m_\alpha} + \frac{1}{2}\sum_\beta \sum_{j\in\beta,\, j\beta\neq i\alpha} \phi_{i\alpha,j\beta}, \tag{7b}$$

$$\mathbf{F}_{i\alpha,j\beta}=-\frac{\partial\phi(r_{i\alpha,j\beta})}{\partial\mathbf{r}_{i\alpha}}, \tag{7c}$$

where $\phi(r_{i\alpha,j\beta})=\phi_{i\alpha,j\beta}$ is the pair potential and the summation Σ_i^α is taken over the particles i belonging to species α.

The microscopic diffusive current of species α, measured in the frame moving with the streaming velocity $\mathbf{u}$ (comoving frame), is

$$\mathbf{J}_\alpha=\frac{1}{V}\sum_i^\alpha m_\alpha\left[\frac{\mathbf{p}_{i\alpha}}{m_\alpha}-\mathbf{u}\right]=\frac{N_\alpha m_\alpha}{V}(\mathbf{u}_\alpha-\mathbf{u}), \tag{8}$$

where $\mathbf{u}_\alpha$ is the mean velocity of species α,

$$\mathbf{u}_\alpha=\frac{1}{N_\alpha}\sum_i^\alpha\frac{\mathbf{p}_{i\alpha}}{m_\alpha}, \tag{9}$$

and

$$\mathbf{u}=\frac{\sum_\alpha N_\alpha m_\alpha\mathbf{u}_\alpha}{\sum_\alpha N_\alpha m_\alpha} \tag{10}$$

is the instantaneous barycentric velocity. Let us define an ''interdiffusive'' current $\mathbf{J}_D$, which we will use in our equations of motion, as

$$\mathbf{J}_D=\frac{1}{V}\left[x_2\sum_i^1\frac{\mathbf{p}_{i1}}{m_1}-x_1\sum_j^2\frac{\mathbf{p}_{j2}}{m_2}\right]=\left[\frac{x_2}{m_1}+\frac{x_1}{m_2}\right]\mathbf{J}_1, \tag{11}$$

where $x_\alpha=N_\alpha/N$ is the number concentration of species α, and we made use of $\Sigma_k\mathbf{J}_k=0$, easily verified from Eq. (8).

The microscopic Irwing-Kirkwood expression for $\mathbf{J}_E$ is [10]

$$V\mathbf{J}_E=\sum_\alpha\sum_i^\alpha\tilde{e}_{i\alpha}\left(\frac{\mathbf{p}_{i\alpha}}{m_\alpha}-\mathbf{u}\right)+\frac{1}{2}\sum_\alpha\sum_\beta\sum_{i\in\alpha}\sum_{j\in\beta}\mathbf{r}_{i\alpha,j\beta}\mathbf{F}_{i\alpha,j\beta}\left[\frac{\mathbf{p}_{i\alpha}}{m_\alpha}-\mathbf{u}\right], \tag{12}$$

where

$$\tilde{e}_{i\alpha}=\frac{m_\alpha}{2}\left|\frac{\mathbf{p}_{i\alpha}}{m_\alpha}-\mathbf{u}\right|^2+\frac{1}{2}\sum_\beta\sum_{j\in\beta,j\beta\neq i\alpha}\phi_{i\alpha,j\beta} \tag{13}$$

is the total energy of particle $i\alpha$ in the comoving frame.

1. Ideal mixtures

As stated in Sec. II A, there cannot be a fully microscopic expression for the heat flux $\mathbf{J}_Q$. However, for mixtures with equal intermolecular potentials and in general for other ideal mixtures, in the thermodynamic limit, partial enthalpies and therefore the heat flux can be written as phase-space functions [1,2]. The heat flux for ideal mixtures is

$$V\mathbf{J}_Q^{ideal}=\sum_\alpha\sum_i^\alpha e'_{i\alpha}\left[\frac{\mathbf{p}_{i\alpha}}{m_\alpha}-\mathbf{u}_\alpha\right]+\frac{1}{2}\sum_\alpha\sum_\beta\sum_{i\in\alpha}\sum_{j\in\beta}\mathbf{r}_{i\alpha,j\beta}\mathbf{F}_{i\alpha,j\beta}\left[\frac{\mathbf{p}_{i\alpha}}{m_\alpha}-\mathbf{u}_\alpha\right], \tag{14}$$

where $e'_{i\alpha}$ is the total energy of particle $i\alpha$ measured in the comoving frame of the species α [obtained from Eq. (13) by replacing $|\mathbf{p}_{i\alpha}/m_\alpha-\mathbf{u}|$ with $|\mathbf{p}_{i\alpha}/m_\alpha-\mathbf{u}_\alpha|$]. The difference between $\mathbf{J}_Q^{ideal}$ and $\mathbf{J}_E$, once neglected within the linear regime the terms quadratic in $(\mathbf{u}_\alpha-\mathbf{u})$ and taken the thermodynamic limit, can be written as in Eq. (3), with the partial enthalpy of component α replaced by [2]

$$\tilde{h}_\alpha=\frac{\langle e'_\alpha+V(P_\alpha)_{ii}\rangle}{m_\alpha N_\alpha}, \tag{15}$$

where the quantity $(P_\alpha)_{ii}$ is the trace of the ''partial'' pressure tensor. Within this approximation, we can use the definition (5) to calculate the transport coefficients.

Clearly, $\mathbf{J}_Q^{ideal}$ is different from $\mathbf{J}_Q$ given in Eq. (3). Evans and Cummings [11] derived an expression for the heat flux defined in Eq. (3). Sarman and Evans [12,13] compared phenomenological coefficients computed with both fluxes and concluded that the ideal approximation is valid, at least for argon-krypton mixtures. However, we did not make use of the EC heat flux because the link between the set of the corresponding phenomenological coefficients and the experimentally measured cross-coefficients still involves thermodynamic data. Therefore, in practice (or at least without any independent data) it is not possible to get the Soret and Dufour coefficients from the EC algorithm to compare with experiments.

C. Non-Hamiltonian equations and response theory

In Eq. (5), the Soret and the other transport coefficients are written as functions of the phenomenological coefficients $L_{\alpha\beta}$'s. We reported, in the preceding section, some microscopic expressions for energy, heat, and mass fluxes, usually employed in simulations. The connection between these fluxes and the phenomenological coefficients can be made using the Green-Kubo relations [14]

$$L_{\alpha\beta}=\frac{V}{3k_B}\int_0^\infty ds\langle\mathcal{J}_\alpha(s)\cdot\mathcal{J}_\beta(0)\rangle_{eq}, \tag{16}$$

with $\mathcal{J}_\alpha$ a heat or mass flux and k_B the Boltzmann's constant.

Using linear response theory we can relate a nonequilibrium flux to the correlation functions and therefore to the $L_{\alpha\beta}$'s. The non-Hamiltonian NEMD equations of motions can be written as [1,15]

$$\dot{\mathbf{r}}_{i\alpha}=\frac{\mathbf{p}_{i\alpha}}{m_\alpha}+\mathsf{C}_{i\alpha}\mathbf{F}_e(t), \tag{17a}$$

$$\dot{\mathbf{p}}_{i\alpha}=\mathbf{F}_{i\alpha}+\mathsf{D}_{i\alpha}\mathbf{F}_e(t), \tag{17b}$$

where $\mathbf{F}_e(t)$ is the imposed perturbation, $\mathsf{C}_{i\alpha}=\mathsf{C}_{i\alpha}(\Gamma)$ and $\mathsf{D}_{i\alpha}=\mathsf{D}_{i\alpha}(\Gamma)$ are suitable tensors that are phase-space functions and which describe the coupling of the perturbation to the system. If Eqs. (17) preserve the phase-space incompressibility, we apply the response theory in its standard form [16] and get the response in a phase-space function **B** as

$$\langle \mathbf{B}\rangle_t=\beta\int_0^t\langle \mathbf{B}(t-s)\mathbf{O}(0)\rangle_{\mathrm{eq}}\cdot\mathbf{F}_e(s)ds+O(\mathbf{F}_e^2), \quad (18)$$

where the time dependence has to be taken with the field turned off and $\beta=1/k_BT$; Furthermore, we made the hypothesis that $\langle \mathbf{B}\rangle_{\mathrm{eq}}=0$; **O** is the variable that couples with the imposed perturbation, defined as

$$\mathbf{O}=\sum_\alpha\sum_i^\alpha\left[\frac{\mathbf{p}_{i\alpha}}{m_\alpha}\cdot\mathsf{D}_{i\alpha}-\mathbf{F}_{i\alpha}\cdot\mathsf{C}_{i\alpha}\right]. \quad (19)$$

To impose a diffusive perturbation $\mathbf{F}_D(t)$, we choose $\mathsf{C}_{i\alpha}\equiv 0$ for every particle $i\alpha$, and $\mathsf{D}_{i\alpha}\equiv A_\alpha$ with $A_1=x_2$, $A_2=-x_1$. To impose a thermal perturbation $\mathbf{F}_Q(t)$, we choose again $\mathsf{C}_{i\alpha}\equiv 0$ and $\mathsf{D}_{i\alpha}$ to be

$$\mathsf{D}_{i\alpha}=\mathsf{S}_{i\alpha}-\frac{1}{N_\alpha}\sum_k^\alpha\mathsf{S}_{k\alpha}, \quad (20)$$

with (I is the unit tensor)

$$\mathsf{S}_{i\alpha}=e'_{i\alpha}\mathsf{I}+\frac{1}{2}\sum_\beta\sum_{j\in\beta}\mathbf{F}_{i\alpha,j\beta}\mathbf{r}_{i\alpha,j\beta}. \quad (21)$$

Using the defined tensors for diffusive and thermal perturbations, we obtain $\mathbf{O}_D=V\mathbf{J}_D$ and $\mathbf{O}_Q=V\mathbf{J}_Q$. With these definitions we can relate each phenomenological coefficient to a response of the system undergoing one of the specified perturbations, as explicitly shown in Sec. II D.

D. Techniques for response measurement

In this section we specify the form of the external perturbation, $\mathbf{F}_e(t)$, we apply to our system, and discuss the different techniques for the response measurement and the linear coefficients determination. We also add a discussion on such a determination using the usual Green-Kubo relations.

In past NEMD applications, several choices for $\mathbf{F}_e(t)$ can be found, including sinusoidal excitations. To determine the matrix of thermal transport coefficients, two temporal functions are suitable,

$$\mathbf{F}_e(t)=(0,0,\tilde{F}_e)\,\delta(t), \quad e=D,Q, \quad (22a)$$

$$\mathbf{F}_e(t)=(0,0,\overline{F}_e)\,\theta(t), \quad e=D,Q, \quad (22b)$$

which have been chosen along the z axis without loss of generality. For each of them we get a response of the type (18). We do not know *a priori* the explicit analytical form of the response. However, it can be written as a Taylor expansion [17] in the field $\mathbf{F}_e$. Therefore, in order to perform the zero-field extrapolation, we adjust a polynom to our response values, as already done in the literature [18]. We use the chi-squared of the fit as a criterium to select the most appropriate polynomial order. We divide the response by the excitation field, rescale it of an opportune factor [see, for example, Eqs. (24)–(26)], and take a Taylor development, getting the 'normalized' response $R_{\alpha\beta}(t)$,

$$R_{\alpha\beta}(t)=\mathcal{L}_{\alpha\beta}(t)+b_{\alpha\beta}(t)F_e^2+c_{\alpha\beta}(t)F_e^4+d_{\alpha\beta}(t)F_e^6+O(F_e^8) \quad \alpha,\beta=1,Q, \quad (23)$$

where $\mathcal{L}_{\alpha\beta}(t)$, $b_{\alpha\beta}(t)$,$c_{\alpha\beta}(t)$,$d_{\alpha\beta}(t)$ are general functions of time, F_e can be either $\tilde{F}_e$ or $\overline{F}_e$, and $e=D,Q$ for $\beta=1,Q$, respectively. The $F_e\to 0$ limit of the right-hand side of the previous expression is the term $\mathcal{L}_{\alpha\beta}(t)$, which can be an equilibrium correlation function or its integral. Indeed, using a δ-like excitation we get in $\mathcal{L}_{\alpha\beta}(t)$ a correlation function, while with a θ-like one, we get its integral. However, still for δ-like external fields, we can integrate the response over time, thus getting the same general expansion in F_e. This procedure, though simply derivable from response theory, has not yet been exploited in the literature.

For an interval of ''small'' fields we can consider as if we were in the limit $F_e\to 0$ [2,1]; this interval thus defines the ''linear'' region. In this region, we have the following responses to impulse excitations:

$$\langle\tilde{J}_{\alpha z}\rangle_{Q,t}=\beta\tilde{F}_QV\langle\tilde{J}_{\alpha z}(t)\tilde{J}_{Qz}(0)\rangle_{\mathrm{eq}}, \quad (24a)$$

$$\langle\tilde{J}_{\alpha z}\rangle_{D,t}=\beta\tilde{F}_D\left[\frac{x_2}{m_1}+\frac{x_1}{m_2}\right]V\langle\tilde{J}_{\alpha z}(t)\tilde{J}_{1z}(0)\rangle_{\mathrm{eq}}, \quad \alpha=1,Q, \quad (24b)$$

whose time integral we compare with the usual Green-Kubo (16) relations, to obtain

$$\frac{\tilde{L}_{\alpha Q,t}}{T}=\frac{1}{\tilde{F}_Q}\int_0^t ds\langle\tilde{J}_{\alpha z}\rangle_{Q,s}, \quad (25a)$$

$$\frac{\tilde{L}_{\alpha 1,t}}{T}=\frac{1}{\tilde{F}_D\left(\frac{x_2}{m_1}+\frac{x_1}{m_2}\right)}\int_0^t ds\langle\tilde{J}_{\alpha z}\rangle_{D,s}. \quad (25b)$$

$$\alpha=1,Q.$$

Still looking at the linear response, from the above step excitations, we have

$$\frac{\tilde{L}_{\alpha Q,t}}{T}=\lim_{\overline{F}_Q\to 0}\frac{\langle\tilde{J}_{\alpha z}\rangle_{Q,t}}{\overline{F}_Q}, \quad (26a)$$

$$\frac{\tilde{L}_{\alpha 1,t}}{T}=\lim_{\overline{F}_D\to 0}\frac{\langle\tilde{J}_{\alpha z}\rangle_{D,t}}{\overline{F}_D\left(\frac{x_2}{m_1}+\frac{x_1}{m_2}\right)}, \quad \alpha=1,Q. \quad (26b)$$

The expressions (25) and (26), give, when taken with t large enough, the linear coefficients $\tilde{L}_{\alpha\beta}$'s. The limit

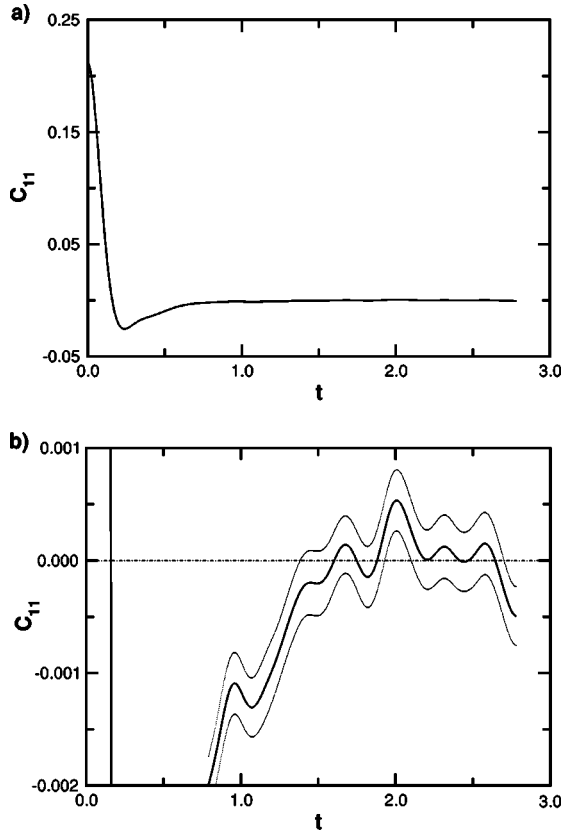

FIG. 1. Correlation function $C_{11}(t)$ for the system 1. (a) The plot of the whole function; (b) the tail.

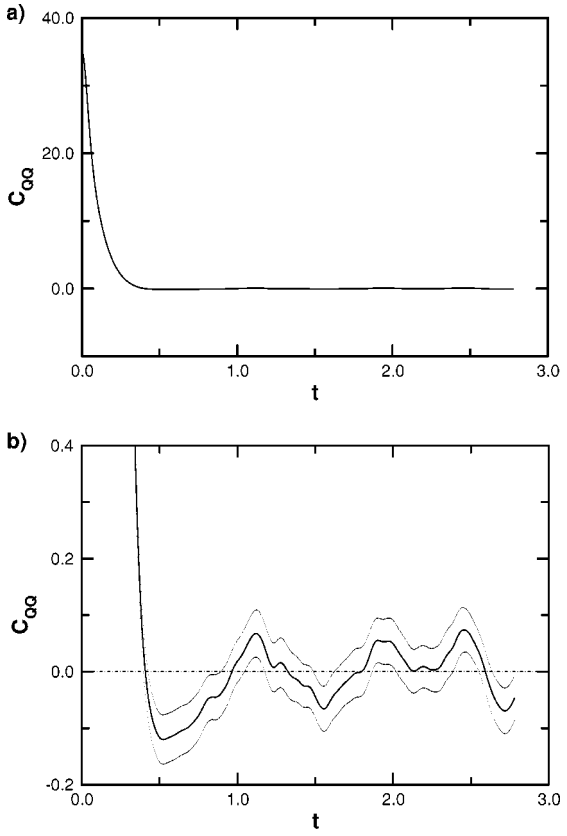

FIG. 2. Correlation function $C_{QQ}(t)$ for the system 1. (a) The plot of the whole function; (b) the tail.

$F_e \to 0$ is usually performed either by choosing a very small value of this field, or by extrapolating to zero field the response values.

There are two conceptually different ways to use expressions (25) and (26). In one of them [19,20], one starts from the well-known Liouville equation

$$\frac{\partial f}{\partial t} = \mathrm{i}L(t) f(\mathbf{\Gamma};t), \tag{27}$$

where $\mathbf{\Gamma}$ is the phase-space vector and f the phase-space distribution function. The solution of Eq. (27) is

$$f(\mathbf{\Gamma};t) = U^{+}(t) f(\mathbf{\Gamma};0), \tag{28}$$

with $f(\mathbf{\Gamma};0)$ chosen to be the equilibrium phase-space distribution function. Formula (28) defines the $U^{+}(t)$ time propagator, adjoint of the time-evolution propagator $U(t)$ acting on the phase-space variables. The out-of-equilibrium average of a flux can therefore be written as

$$J(t) \equiv \langle \mathcal{J}_\eta \rangle_{neq} = \int d\mathbf{\Gamma} f(\mathbf{\Gamma};t) \mathcal{J}_\eta(\mathbf{\Gamma}) \equiv (\mathcal{J}_\eta, U^{+}(t) f_0) = (U(t)\mathcal{J}_\eta, f_0), \tag{29}$$

where $\mathcal{J}_\eta(\mathbf{\Gamma})$ is the phase-space function corresponding to the flux $\mathcal{J}_\eta$. Equation (29) is fundamental to approach nonequilibrium statistical mechanics. It says that for systems initially at equilibrium, nonequilibrium averages of an observable can be obtained as averages of the observable, evoluted in time under the full (perturbed) dynamics, over the equilibrium (initial-time) ensemble. The method based on Eq.

TABLE I. Conditions for the experiments (expt.) and simulations (sim., $N=108$) for the two thermodynamical points studied. The molar fraction is denoted with $x_{Ar,Kr}$ and mass fraction with $w_{Ar,Kr}$; ρ is the mass density of the mixture, P the pressure, and T the temperature.

System	P (atm)	T (K)	N_{Ar}	x_{Ar}	w_{Ar}	ρ (g/cm^3)	r_s	r_c
1, expt.	<3	95.2 ± 2.4		0.6790	0.5020			
1 sim.	1	95.2 ± 0.1	73	0.6759	0.4985	1.8119	2.35	$L/2$
2 expt.	<3	93.0 ± 2.4		0.7840	0.6340			
2 sim.	1	93.0 ± 0.2	85	0.7870	0.6379	1.6734	2.35	$L/2$

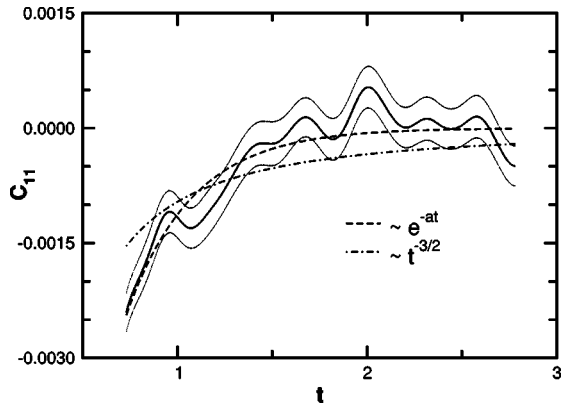

FIG. 3. Tail of the correlation $C_{11}(t)$ for the system 1, with two different fits.

(29) is generally called *dynamical approach* and can use any type of time dependence of the external perturbation.

In contrast to this, the *stationary approach* [1,21] uses time averages over the stationary state, attained when one chooses a θ-like perturbation in conjunction with a thermostat which removes the dissipated heat. We stress that this approach only allows the calculation of the phenomenological coefficient, without giving any information on the dynamical (transient-time) behavior.

In the case of *dynamical approach*, the subtraction technique [19] for noise reduction has been already proposed in order to have a significant signal-to-noise ratio. However, it is known that this technique is suitable only at short times. For correlation function showing enough long time memory, the noise becomes as large as the natural fluctuation of the measured current. Hence, the ratio of the measured current to the corresponding excitation field, for large enough times, diverges for small values of the field. We will see that this is the situation encountered in our case.

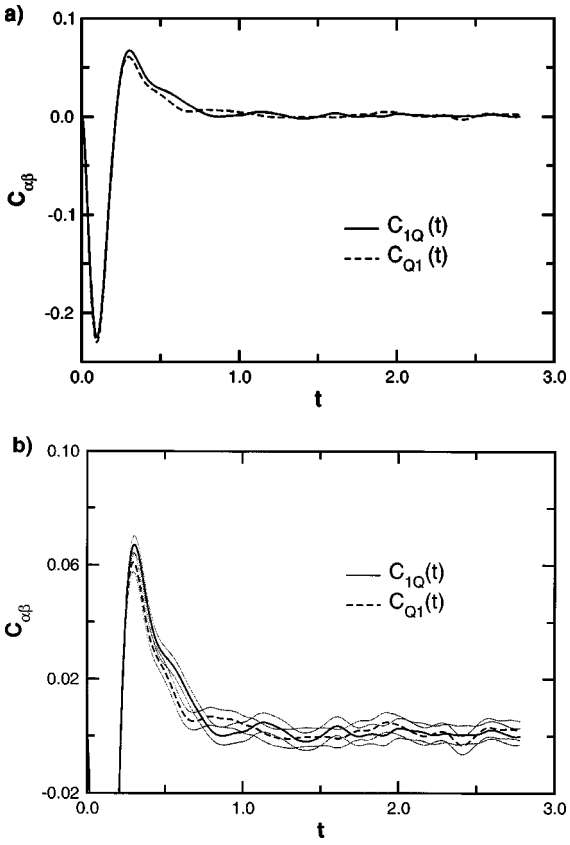

FIG. 4. Cross correlations for the system 1, ensemble *NVT*. (a) the full plot, (b) the plot in a reduced window with averages and statistical errors.

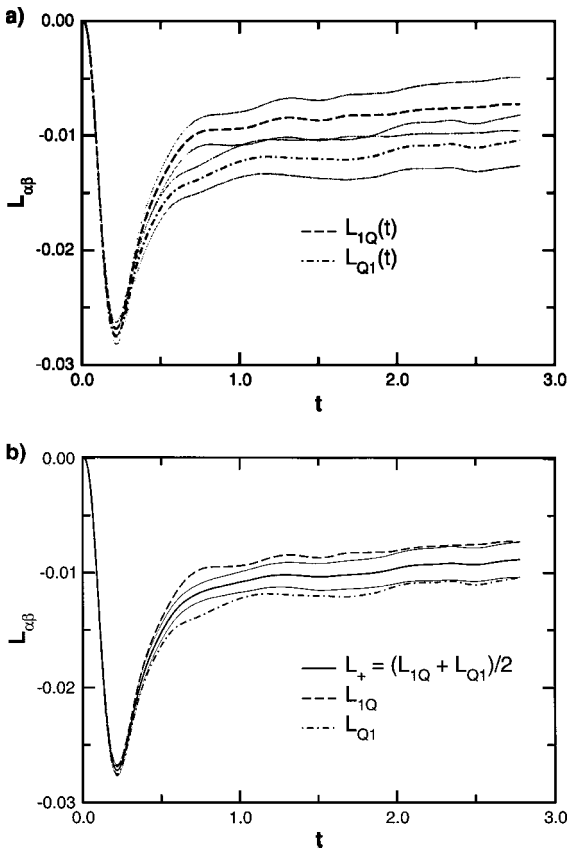

FIG. 5. Integrals of the cross correlation functions for the system 1. (a) $L_{1Q}(t)$ and $L_{Q1}(t)$ are plotted with their statistical errors, (b) $L_{1Q}(t)$, $L_{Q1}(t)$, as well as $L_{+}(t)=[L_{1Q}(t)+L_{Q1}(t)]/2$ with its statistical error.

III. MODELS

We have studied two mixtures of argon-krypton atoms, with masses $m_1=39.944$ and $m_2=83.80$ a.u. The $N=108$ particles system is enclosed in a cubic box of side L and volume $V=L^3$. The model for interactions is a Lennard-Jones potential,

$$\phi_{LJ}^{\alpha\beta}(r)=4\epsilon_{\alpha\beta}\left[\left(\frac{\sigma_{\alpha\beta}}{r}\right)^{12}-\left(\frac{\sigma_{\alpha\beta}}{r}\right)^{6}\right],$$

with parameters $\epsilon_{11}=119.8\ k_B$, $\epsilon_{22}=167.0\ k_B$, $\sigma_{11}=3.405$ Å, $\sigma_{22}=3.633$ Å, and with cross parameters defined by the Lorentz-Berthelot rules

$$\sigma_{12}=\frac{\sigma_{11}+\sigma_{22}}{2},$$

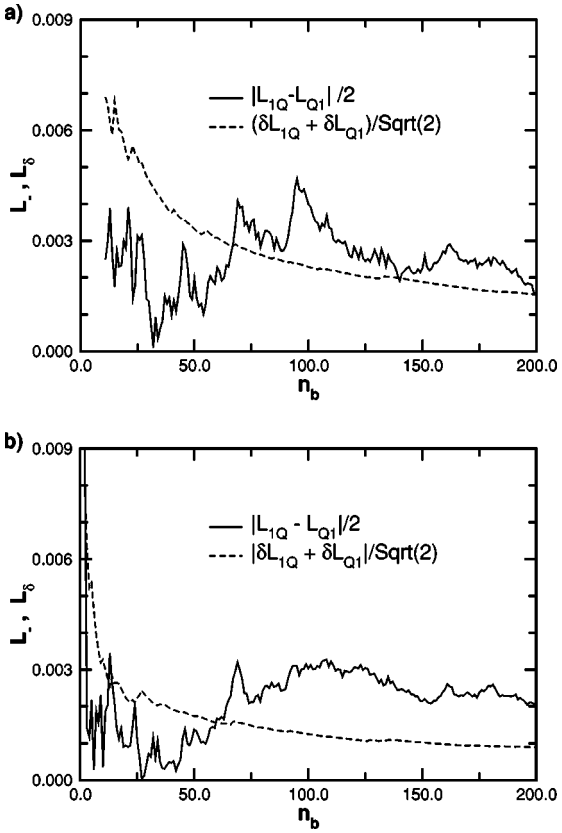

FIG. 6. The quantities $L_-=|L_{1Q}-L_{Q1}|/2$ and $L_\delta=(\delta L_{1Q}+\delta L_{Q1})/\sqrt{2}$ are plotted against the block number n_b, for two different times: (a) at $t=0.72\tau$, where the difference L_- is the most important, (b) at $t=2.32\tau$, where one finds the minimal difference between the two cross coefficients (see Fig. 5).

$$\epsilon_{12}=\sqrt{\epsilon_{11}\epsilon_{22}}.$$

Units are σ_{11} for length, ϵ_{11} for energy, and $\tau=(m\sigma_{11}^2/\epsilon_{11})^{1/2}=2.156$ ps for time. All the quantities will be quoted in such units, unless explicitly mentioned. To avoid discontinuities in the integration of equations of motion, we modify the model so that the new potential function $\phi^{\alpha\beta}$ gives pair forces $|\mathbf{F}_{i\alpha,j\beta}|$ which go to zero in a continuous way at the edge of the box. This is obtained by matching a spline with a cubic line, such as to satisfy the conditions

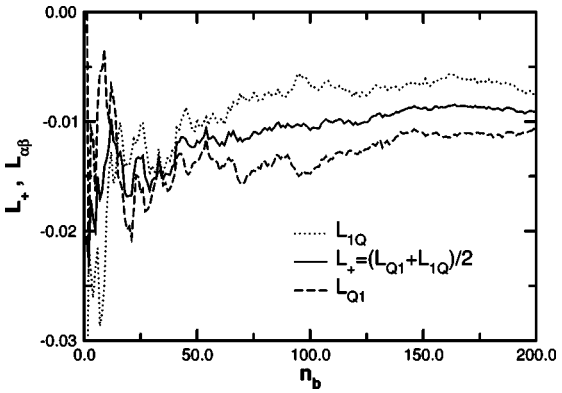

FIG. 7. The quantity $L_+(t)=[L_{1Q}(t)+L_{Q1}(t)]/2$ plotted against the block number.

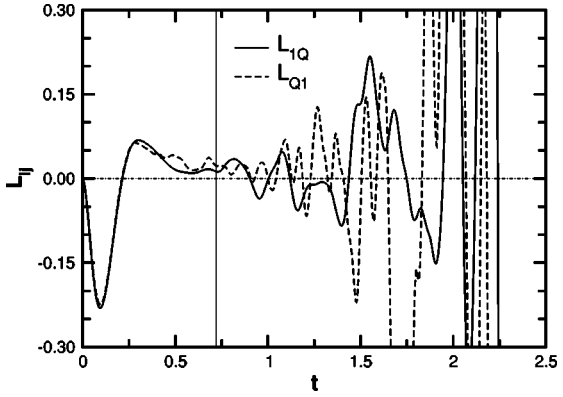

FIG. 8. The two cross coefficients L_{1Q} and L_{Q1} for system 1. The vertical line shows the time window used to get the converged time integrals in Ref. [2].

$$\frac{\partial^2\phi^{\alpha\beta}(r_s)}{\partial r^2}=\frac{\partial^2\phi_{LJ}^{\alpha\beta}(r_s)}{\partial r^2}, \tag{30a}$$

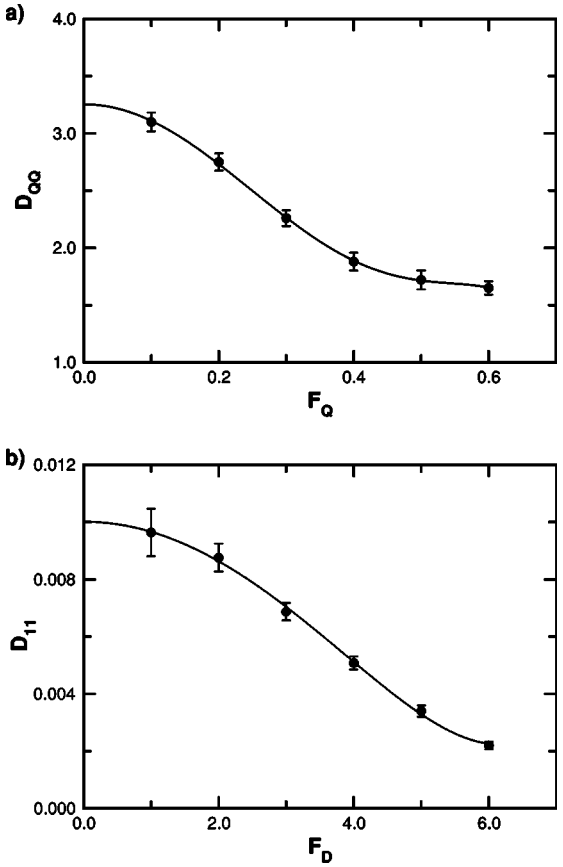

FIG. 9. Direct responses to a δ-like excitation of (a) heat and (b) mass, for different perturbation strengths.

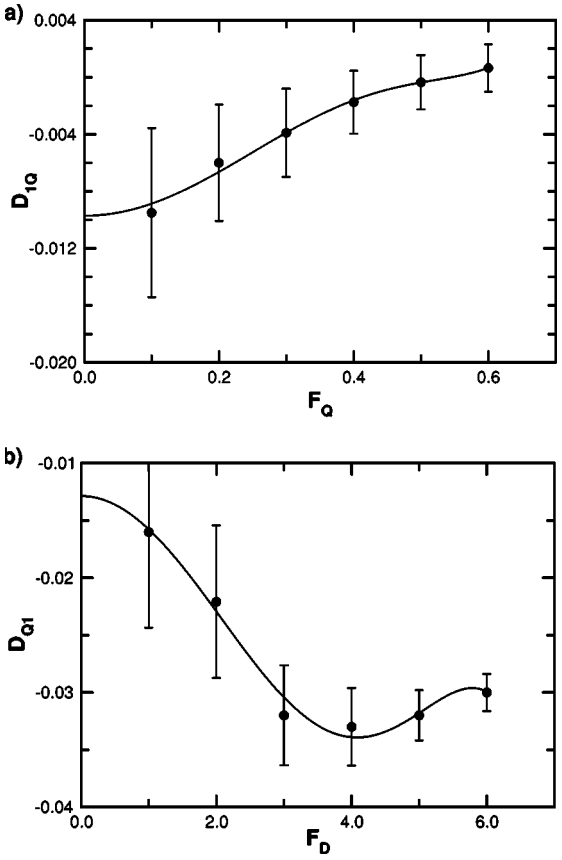

FIG. 10. Cross responses to a δ-like excitation of (a) heat and (b) mass, for different perturbation strengths.

$$\frac{\partial \phi^{\alpha\beta}(r_s)}{\partial r} = \frac{\partial \phi^{\alpha\beta}_{LJ}(r_s)}{\partial r}, \tag{30b}$$

$$\frac{\partial^2 \phi^{\alpha\beta}(r_c)}{\partial r^2} = 0, \tag{30c}$$

$$\frac{\partial \phi^{\alpha\beta}(r_c)}{\partial r} = 0, \tag{30d}$$

where r_s is the radius where the Lennard-Jones potential is cut, and r_c is the one where the spline ends. The potential $\phi^{\alpha\beta}(r)$ is the integral over r of the pair force $\partial\phi^{\alpha\beta}(r)/\partial r$ with the condition that $\phi^{\alpha\beta}(r)=0$ for $r \geqslant r_c$. Our boundary conditions are periodic in all directions. We integrated the equations of motion (17) using the velocity Verlet algorithm, with a slight modification at the beginning of each NEMD trajectory, due to the impulsive perturbation employed [19,22]. The time step is whenever $h=5$ fs, unless otherwise declared. We performed calculations both in NVE and in NVT ensembles. For the latter we used the Nosé-Hoover thermostat whose inertia parameter $Q=0.5$ kJ mol^{-1} ps^2 has been chosen following the procedure used in Ref. [23]. That is, the value has been adjusted by trial and error, performing a number of dynamical NEMD runs and choosing the largest value consistent with a temperature control effective over the short time span of the observed stationary part of the dynamical response of the system.

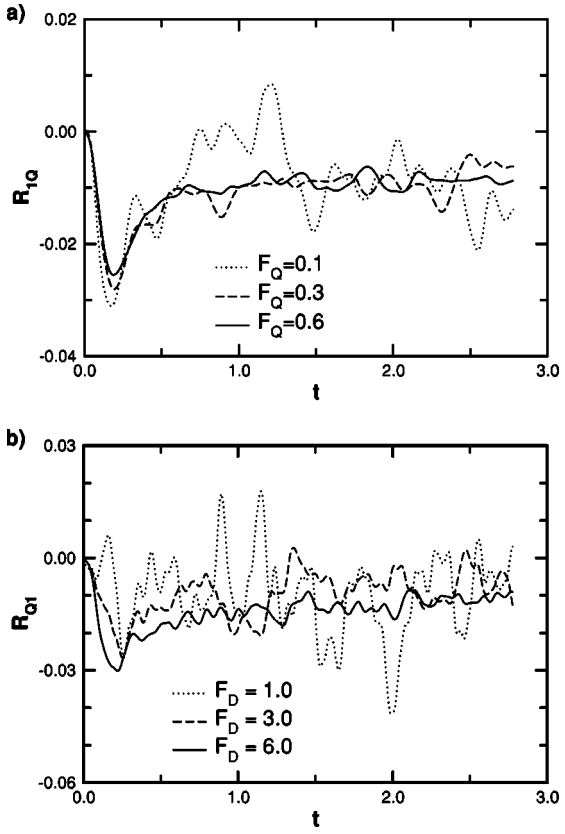

FIG. 11. Responses R_{1Q} and R_{Q1} to a step function excitation for several perturbation strengths.

We tested our code by performing simulations on the system of PC, which is very close to that of ME. We found results that agree well within the statistical error bars. Furthermore, it is worth noting that this work presents results obtained by two independently developed codes (a sequential and a parallel one, running respectively on SGI or HP, and Cray T3E) which give the same results at any time of corre-

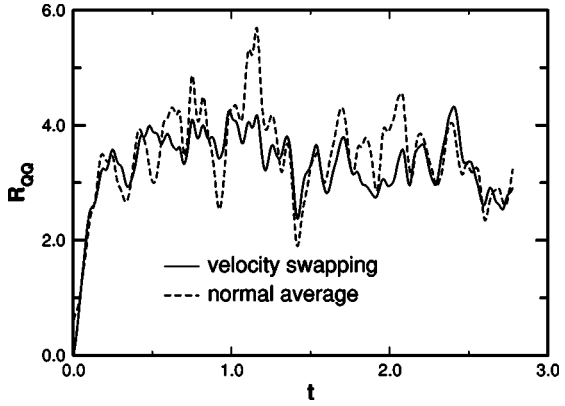

FIG. 12. Two reponses R_{QQ} for a step function excitation with strength out of the linear region. The two curves correspond to an average over 20 initial configurations. For one of the two curves, we used 10 initial configurations and another 10 were created by velocity inversion of the former ones.

TABLE II. Results for the GK simulations, systems 1 and 2. The total simulation time for each point is 60 ns.

State	Ens.	L_{QQ}	$10^2 L_{1Q}$	$10^2 L_{Q1}$	$10^2 L_{+}$	$10^2 L_{11}$
1	NVT	3.37 ± 0.09	-0.76 ± 0.48	-1.073 ± 0.48	-0.92 ± 0.30	1.009 ± 0.027
1	NVE	3.50 ± 0.25	-1.37 ± 0.50	-1.40 ± 0.50	-1.39 ± 0.31	1.027 ± 0.060
2	NVT	3.37 ± 0.07	-0.76 ± 0.42	-0.90 ± 0.54	-0.83 ± 0.30	0.980 ± 0.016
2	NVE	3.33 ± 0.08	-0.88 ± 0.45	-0.80 ± 0.45	-0.84 ± 0.34	0.960 ± 0.03

lation functions, up to the last significant digit.

The experimental conditions are those of Refs. [5,6], and are reported in Table I together with those of the simulations. In the experimental work cited, the pressure is not reported. We got the pressure value from J. C. Legros by private communication. We performed NPT simulations to prepare our simulation system. In Table I, we also give the average density of the NPT simulations.

IV. RESULTS OF THE COMPUTATIONS

We report here the results of NEMD simulations. Other methods, e.g., boundary-driven NEMD [21,24,25], were not possible in our case, since the liquid-vapor coexistence region for argon and krypton is too close to the studied state points, and therefore the mixture would undergo a phase transition when submitted to important temperature gradients.

As stated in Sec. II D, we can divide the NEMD techniques into dynamical and stationary ones, that is into techniques that measure the transient responses and techniques that measure the stationary response. We report, in the following, results for both classes of techniques.

A. Dynamical techniques

1. Green-Kubo

We performed Green-Kubo calculations over a continuous trajectory, divided into $n_b = 200$ blocks, each of 300 ps. This corresponds to a total accumulation time of 60 ns; this length is around four times longer than that of Ref. [4] (16 ns) for a similar calculation. For a block, say b, we calculate the time correlation functions, the $C^b_{\alpha\beta}(t)$'s, and their time integrals, the $L^b_{\alpha\beta}(t)$'s. We then calculate averages and standard errors

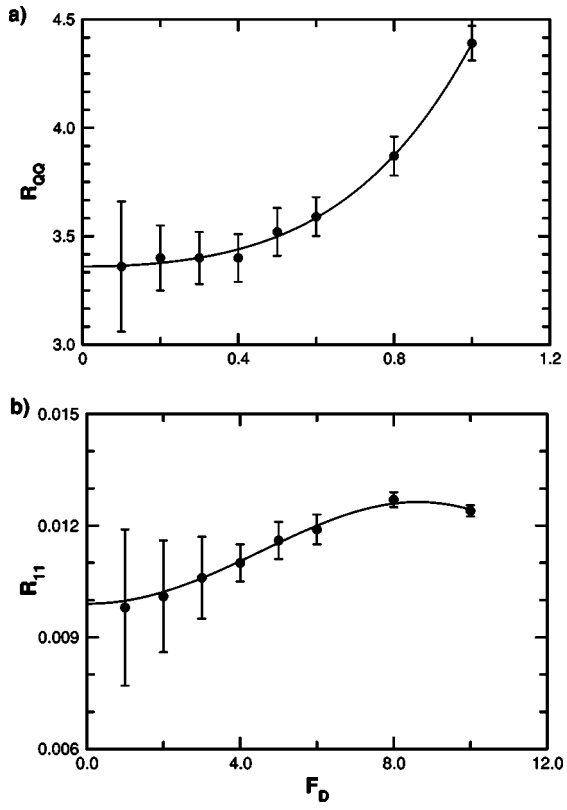

FIG. 13. Dynamical direct responses to a step function excitation as a function of the imposed field. System 1, constant density and temperature.

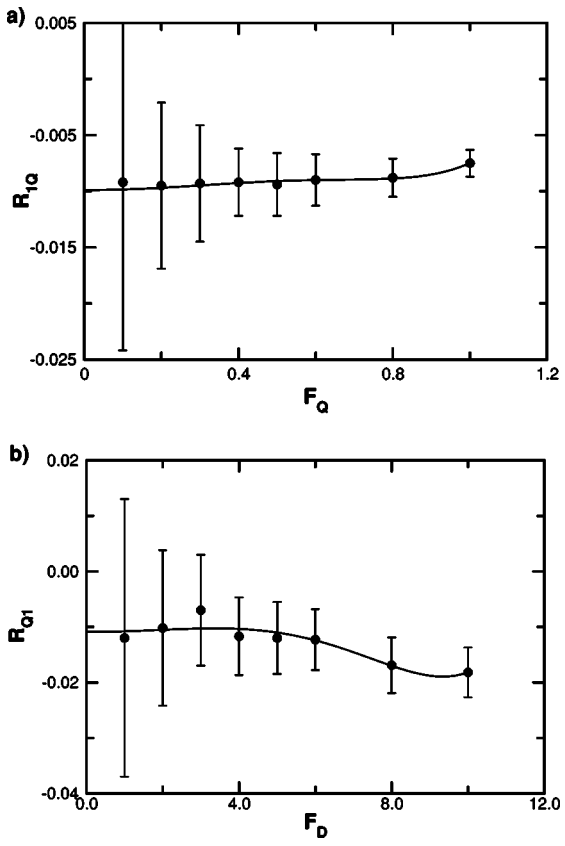

FIG. 14. Dynamical cross responses to a step function excitation as a function of the imposed field. System 1, constant density and temperature.

TABLE III. Phenomenological coefficients obtained by NEMD simulations, systems 1 and 2.

Syst.	Method	L_{QQ}	$10^2 L_{1Q}$	$10^2 L_{Q1}$	$10^2 L_{11}$
1	NEMD δ	3.30 ± 0.07	-0.96 ± 0.50	-1.30 ± 0.80	1.02 ± 0.01
1	NEMD θ dyn.	3.36 ± 0.10	-0.99 ± 0.19	-1.0 ± 1.0	0.99 ± 0.06
1	NEMD θ stat	3.34 ± 0.07	-1.00 ± 0.17	-0.99 ± 0.62	1.01 ± 0.04
2	NEMD θ stat	3.31 ± 0.07	-0.82 ± 0.18	-0.89 ± 0.58	0.97 ± 0.03

on the whole set of block values, hence the correlation functions $C_{\alpha\beta}(t)$'s and their time integrals $L_{\alpha\beta}(t)$'s, as

$$\mathcal{A}(t) = \frac{1}{n_b} \sum_{b=1}^{n_b} \mathcal{A}^b(t) \qquad \mathcal{A} = C_{\alpha\beta}, L_{\alpha\beta}. \tag{31}$$

If one *supposes* that the blocks give statistically independent values for the correlation functions, then the standard error is given by the expression

$$\delta\mathcal{A}(t) = \frac{1}{\sqrt{n_b}} \left\{ \frac{1}{n_b - 1} \sum_{b=1}^{n_b} [\mathcal{A}^b(t) - \mathcal{A}(t)]^2 \right\}^{1/2}. \tag{32}$$

In Figs. 1 and 2 we report the direct correlation functions $C_{11}(t)$ and $C_{QQ}(t)$ for the system 1. We note that $C_{11}(t)$ has not yet decayed up to 2τ. For the cross correlation the calculation of the decay time is obviously more difficult. We therefore decided to use one of $C_{11}(t)$ as the decay time of all correlations. The function $C_{11}(t)$ does not show any evidence of a $t^{-3/2}$ long time tail behavior, as it is clear by looking at Fig. 3. From this figure we also see that we can consider the correlation function as decayed at times between 2.2 and 2.5τ; we take the decay time $t_c \approx 2.3\tau$. This value is more than two times larger than the one used in previous works [2,4] on Ar-Kr mixture. As for the cross correlations, they are reported in Fig. 4, while in Fig. 5 we report their integrals, together with the mean integral

$$L_+(t) \equiv [L_{1Q}(t) + L_{Q1}(t)]/2.$$

We stress that there is a significative difference between the two cross correlation functions even at short times. In

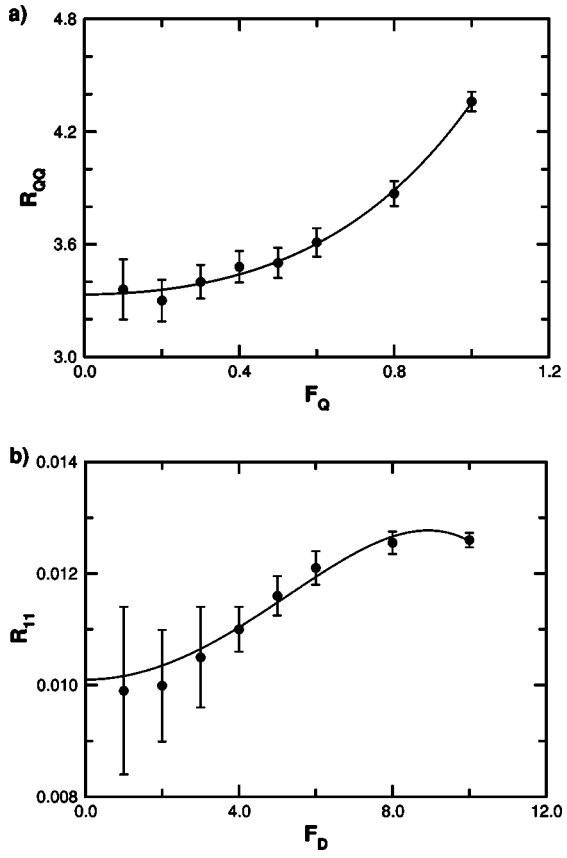

FIG. 15. Stationary direct responses to a step function excitation as a function of the imposed field. System 1, constant density and temperature.

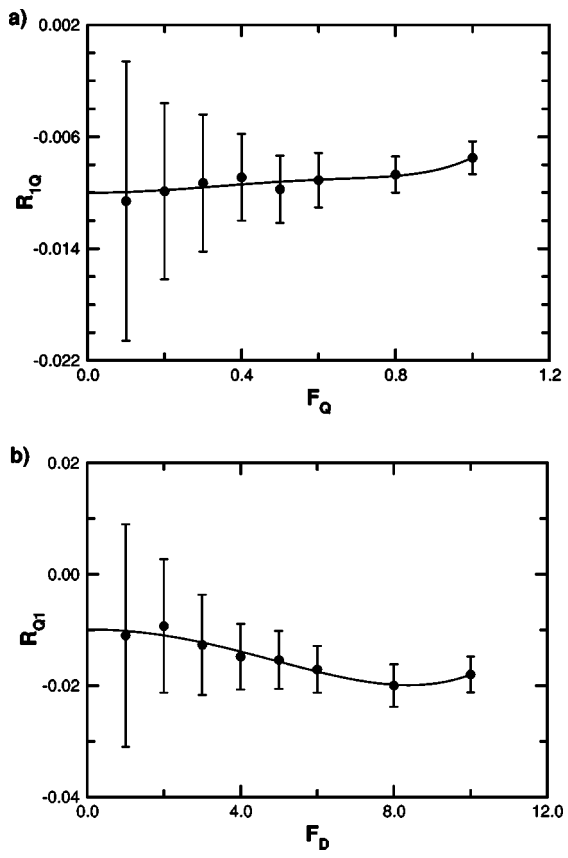

FIG. 16. Stationary cross responses to a step function excitation as a function of the imposed field. System 1, constant density and temperature.

TABLE IV. Simulation results, as averaged over all obtained values (with different methods); systems 1 and 2.

Syst.	L_{QQ}	$10^2 L_{1Q}$	$10^2 L_{Q1}$	$10^2 L_{+}$	$10^2 L_{11}$
1	3.374 ± 0.034	-1.016 ± 0.099	-1.153 ± 0.083	-1.084 0.083	1.0112 ± 0.0063
2	3.340 ± 0.030			-0.835 ± 0.128	0.9701 ± 0.0142

particular, we notice that the difference between the two cross correlations is larger than the sum of the two correlations' errors divided by $\sqrt{2}$,

$$|L_{1Q} - L_{Q1}| > \frac{\delta L_{1Q} + \delta L_{Q1}}{\sqrt{2}},$$

as one can see from Fig. 6 for two different times. We recall that the two cross correlation functions must be equal. We therefore conclude that we do not estimate well the variance, that is the blocks are not statistically independent. To integrate the previous analysis, we plotted L_{+} against the block number, on Fig. 7. We see that the function L_{+} has a slow convergence rate, and L_{1Q}, L_{Q1} are still a little different after 200 blocks. Altogether these results indicate that the blocks are not yet long enough to be completely independent while their number should be further increased to have full convergence. In any event, even so, we can consider to have accumulated enough statistics to get reliable significant results.

In Table II the results for the phenomenological coefficients are reported, for both NVT and NVE calculations and for both the studied state points. We stress that NVT and NVE simulations are in very good agreement with each other. Besides the results in Table II, this is seen comparing the first parts of the correlation functions, which are not noisy, with each other.

2. Dynamical, impulsive NEMD

We performed NEMD simulations using the subtraction technique and the impulsive excitation, for the system Ar-Kr 1. In the linear regime, the responses are proportional to correlation functions as in Eqs. (24), whose integrals are related to phenomenological coefficients through Eq. (25b). We found that the correlation functions converge only for long times, i.e., at around 4–5 ps, as in the GK case. It is known [26] that, at these times, the exponential decorrelation between the equilibrium and nonequilibrium trajectories makes the subtraction technique unable to yield the zero field limit with reasonable accuracy. This is shown, in our case, in Fig. 8, where the calculated $L_{1Q}(t)$ and $L_{Q1}(t)$ for $\tilde{F}_Q = 0.01$ and $\tilde{F}_D = 0.2$, respectively, are plotted. One clearly sees the exponential divergence at long times. The vertical line defines the time window used to get the converged time integrals in Ref. [2]. For such times, with the performed statistics, the substraction technique still gives good accuracy, but in our case the convergence has not yet been attained. We conclude that, in our case, the subtraction technique cannot be directly useful for such calculations. Nevertheless, for short times, it gives a clear confirmation of the Onsager reciprocal relations in the linear regime.

Out of the linear regime, we expect to have an appreciable improvement of the signal-to-noise ratio. We performed simulations for several field values out of the linear region, i.e., $\tilde{F}_Q \in [0.1, 0.6]$ and $\tilde{F}_D \in [1, 6]$. We accumulated data over a total simulating time of 12 ns for each value of the fields, therefore the total time for the whole set of points is 72 ns. We have then integrated the response, and determined the plateau value of the integrals.

The dynamical technique allows us to see the modification of the correlation function's form with the value of the imposed field. We report in the Appendix the study of the change of this form as function of the imposed field strength. We study also in the Appendix the validity of the ORR out of the linear region. This is seen as well in the converged integrals, as in the remainder of this section.

All the responses converge between 2.0 and 2.5τ. We took a weighted average of the integrals' values within this time window, and plotted them against the imposed field strengths, as in Figs. 9 and 10. A polynomial, weighted fit (see Sec. II D) has been performed, and the zero field limit of the responses has been determined. The obtained chi-squared values correspond to a probability (to obtain such fits) of around 98% for all the fits. The results are in Table III. They are consistent with the Green-Kubo determinations. The errors on the cross coefficients are, however, large, in slight contrast to the previous situation. This means that the points are not very well fitted by the imposed polynomial function.

TABLE V. Experimental and simulation results for the mixture Ar-Kr, systems 1 and 2. The errors correspond to two times the standard deviation. The total length of the simulation is Δt.

Syst.	Method	Δt (ns)	10λ (W/K m)	$10^9 D$ (m^2/s)	$10^{11} D_T$ (m^2/K s)	$10^2 S_T$ (1/K)
1	Sim.	335	1.031 ± 0.022	1.307 ± 0.018	2.93 ± 0.50	2.24 ± 0.40
1	Expt.					2.78 ± 0.66
2	Sim.	120	1.067 ± 0.018	1.337 ± 0.019	2.77 ± 0.54	2.07 ± 0.69
2	Expt.					2.10 ± 0.32

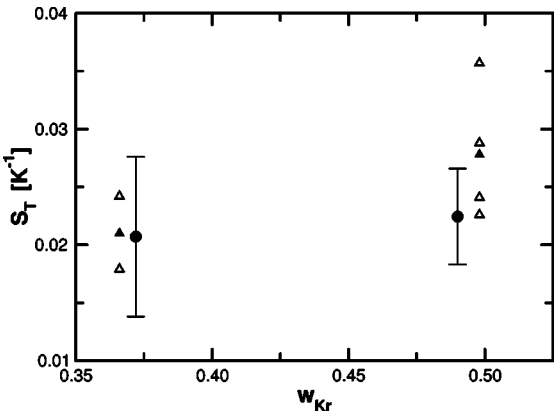

FIG. 17. Comparison between experiments [5] and simulation (this work), for two states of the Ar-Kr mixture. The values of the simulation are calculated over all the results obtained by EMD and NEMD and reported with two standard deviations error. They are at the same argon mass fraction as the experiments, but have been shifted in the plot for better readability.

The Onsager reciprocity relations are verified in the linear regime, but not out of this regime. This is clearly indicated by looking at the progression of the two responses against the field (Fig. 10): they have opposite trends. Note, however, that, in the nonlinear region, the responses have not any longer a direct physical meaning.

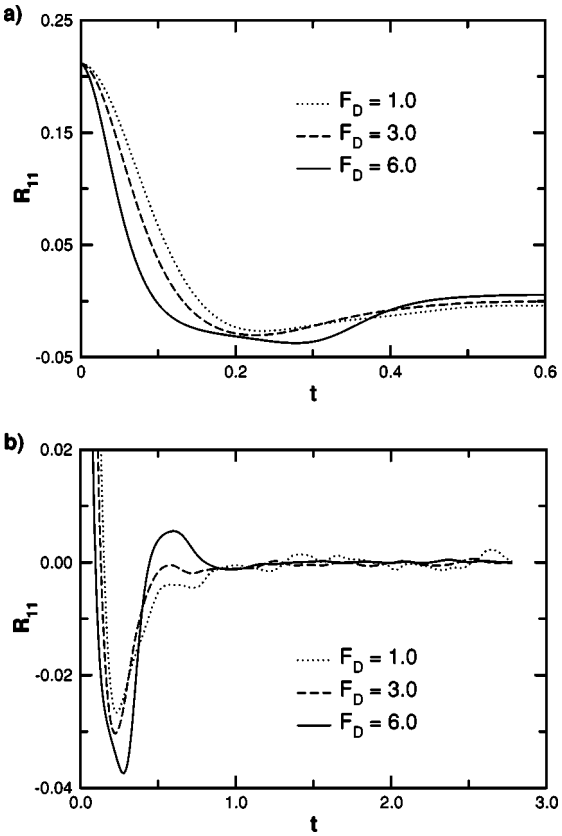

FIG. 18. Direct response to a δ-like mass perturbation for different field strengths. (a) Short time response; (b) tail response.

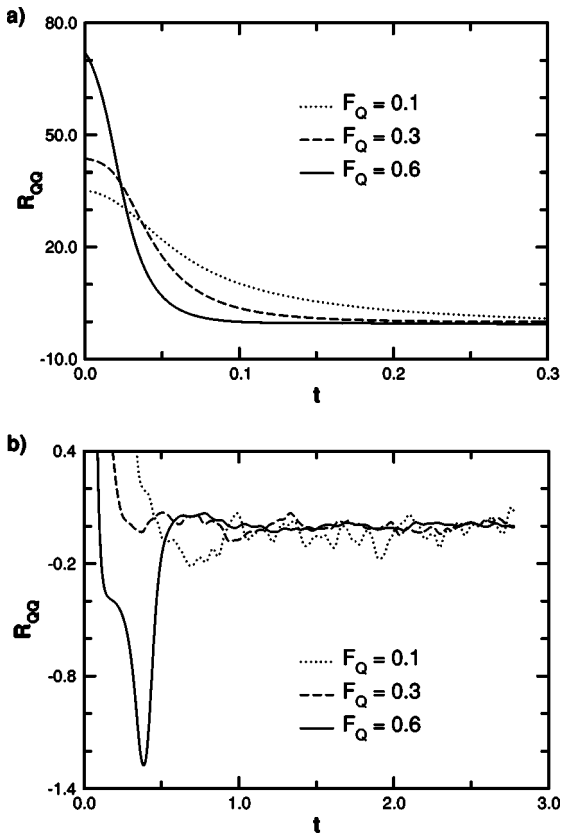

FIG. 19. Direct response to a δ-like heat perturbation for different field strengths. (a) Short time response; (b) tail response.

3. Dynamical, step-function NEMD

We performed simulations with the step-function excitation (see Sec. II D) for different strengths, in and out of the linear region. In the linear region, simulations proved however to give too noisy signals, so that it was impossible to extract the converged values. This is not surprising, since we are continuously disturbing the system, therefore this technique is even more noisy than the δ-like one. As for the simulations out of the linear region, we did not use the subtraction technique, because here the response is much more important than the signal at equilibrium, therefore, this technique would increase the statistical error ($\sigma \approx \sigma_{neq} + \sigma_{eq}$) without improving the response. However, to get a neater signal, we used the technique proposed by Evans [16] which consists in the creation, for each equilibrium starting configuration, of a configuration with opposite velocities; we averaged on the entire set of responses obtained starting from these two set of configurations. This gives a significative reduction of the statistical noise, around a factor 2, as shown in Fig. 12.

Despite this noise reduction technique, the cross reponses at low (nonlinear) fields prove still too much noisy to extract a useful information. In Fig. 11 we plotted the cross reponses for three different values of the external field, each coming from a simulation of around 12 ns. The figure shows that it is not possible to distinguish the convergence of the curves, though the field values are already out of the linear region. Moreover, for the heat reponse to a mass excitation, we have

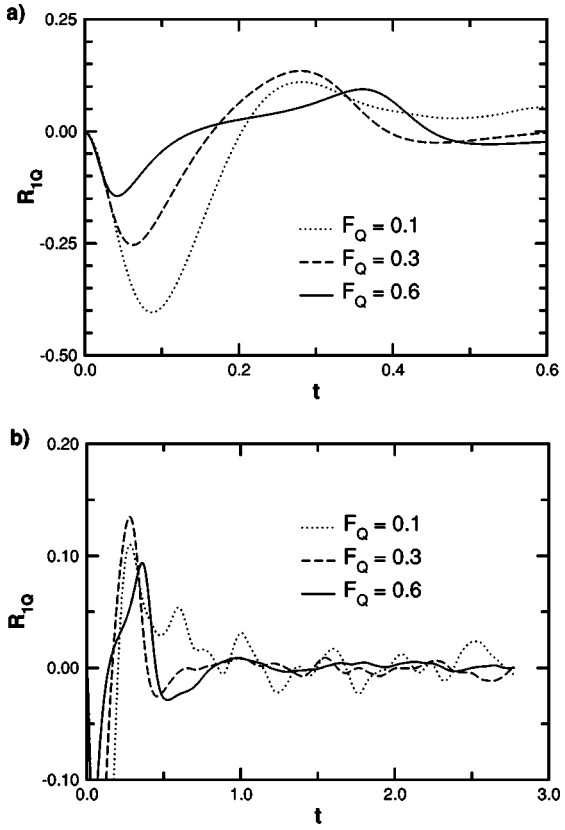

FIG. 20. Cross response to a δ-like heat perturbation for different field strengths. (a) Short time response; (b) tail response.

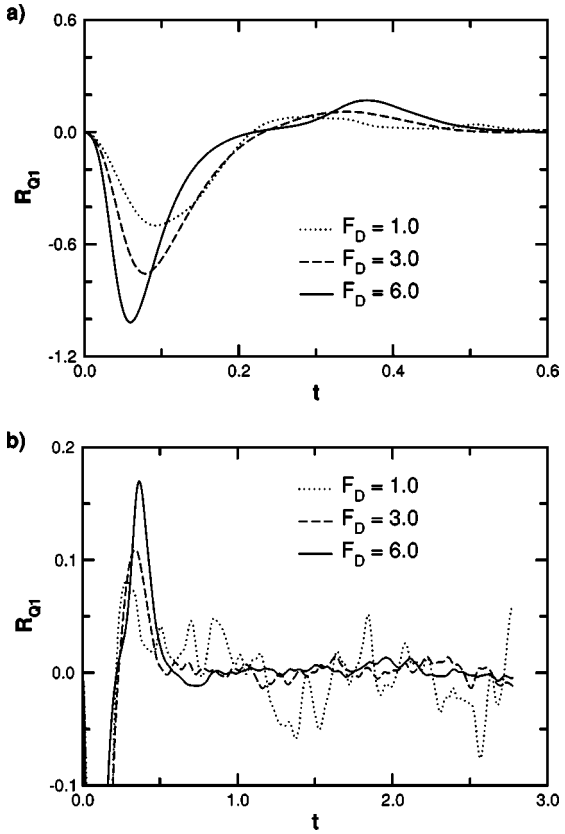

FIG. 21. Cross response to a δ-like mass perturbation for different field strengths. (a) Short time response; (b) tail response.

much more noise than with the other cross signal. This is not surprising, since the heat observable contains several different variables as forces, velocities, positions and therefore undergoes larger fluctuations.

However, if one increases the intensity of the excitation, one begins to find neater responses. We went up to $F_Q=1$ and $F_D=10$. It is possible to go besides these values, but our implementation of the Nosé-Hoover thermostat would ask a too small time step. On Figs. 13 and 14 we report the progression of the reponses as nonlinear functions of the applied field. In Table III there are the results of the zero field extrapolation of the integrated reponses, i.e., the phenomenological coefficients. They are in good agreement with each other and with the determinations from other methods.

B. Stationary technique

We performed simulations with θ-like excitation for several field values, at the edge or out of the linear region, i.e., $\overline{F}_Q \in [0.1,1]$ and $\overline{F}_D \in [1,10]$. We accumulated data over a total simulation time of 12 ns for each value of the field, using the time step $h=5$ fs, apart for the strongest fields, for which it has been reduced to 2 fs. In Figs. 15 and 16 we report the responses as functions of the imposed field together with their best fits. For all the fits we had chi-squared values that correspond to 99% of fit probability.

From the fits we see that the Onsager's reciprocal relations are verified in the linear region, while they are not out of this region, as it was the case for dynamical δ-like NEMD technique.

The phenomenological coefficients' determination is in good agreement with GK, as seen comparing values in Table III with those of Table II.

C. Comparison of simulation results with experiments

In order to make a better comparison between the methods, we have performed an average over all the simulation values, calculating the variance by combining the various variances. This is correct for the system 1, because we have many different values for the coefficients. For system 2 much less individual responses were studied, thus we reported only the statistics on direct coefficients, which we expect correct, and for the coefficients L_+ as calculated from all the available cross coefficents' values. The results are reported in Table IV. Looking at the results obtained with the different techniques in the preceding sections, we can draw the following conclusions.

(i) The results from GK and the different NEMD techniques are in good agreement with each other. The direct phenomenological coefficients of system 1 agree within 1%, while the more noisy cross coefficients agree within 10%, as given by standard deviations in Table IV. This agreement refers to a total simulation time of around 0.3 μs. For system 2, we have larger values of the variance, i.e., 15% for the cross coefficient L_+. This is due to the fact that we averaged on fewer values and on a shorter simulation time, 0.19 μs.

(ii) Both Green-Kubo and NEMD cross coefficients determinations are found to have slower convergence than expected when looking at previous works on the subject [1,2,4]; they have, however, comparable performances. Indeed, for some NEMD determinations we have a significantly smaller error than for GK, but NEMD simulations have been carried on for a longer time. Moreover, one has to take into account the time needed to create the initial (equilibrium) configurations.

(iii) The Onsager reciprocity relations are found valid in the linear region. Out of this region, they are no more verified, as one can see from the dynamical and stationary NEMD responses (see Figs. 10, 14, and 16).

We showed that convergence is slow for all techniques. For comparison with the experiments, we therefore used the averaged values given in Table IV. We calculated the transport coefficients λ, D, D_T, S_T in the mass reference frame, as indicated in Table V.

In Fig. 17 the coefficients S_T calculated by simulation show a very good agreement with experimental data.

V. CONCLUSION

In this paper we performed equilibrium and nonequilibrium calculations in order to compute the Soret coefficient for two state points of the argon-krypton mixture, experimentally measured. As statistical errors in equilibrium GK simulations are independent of the system size [26], a very small system (108 particles) was chosen in order to compare the efficiency of GK and NEMD calculations.

The matrix of phenomenological coefficients has been obtained by various techniques which differ in the use of δ- and θ-like excitations in the linear and nonlinear regime, assuming the ideal mixture approximation for the heat flux. We found that the linear dynamical NEMD (performed through subtraction technique) cannot be used in our case, and in general when the response does not decay within ~ 1 ps, because of the exponential divergence of trajectories. Nonlinear dynamical and stationary NEMD, for which we used θ-like and δ-like perturbations, give reliable results in good agreement with each other. However, in spite of the long total simulation time for each technique (60–100 ns), important statistical errors are found (from 17% to 50%), in contrast with previous works on the subject. We had also the occasion to study the validity of Onsager reciprocal relations out of the linear regime. We found that the cross responses are not any longer equal in this regime.

We confirmed our NEMD results by comparison with Green-Kubo calculations, that we carried on during a trajectory of 60 ns. As a result of this long simulation, we found a very slow convergence for both cross coefficients, which are hence determined with modest accuracy (around 30%). Green-Kubo calculations give performances comparable to the NEMD ones.

A comparison between simulations and experiments has been attempted. The common enthalpy-diffusion-free expression for the heat flux has been chosen. The comparison of the simulations with experiments for the Soret coefficient is very good and this suggests that the heat flux choice is correct. This is also confirmed by recent work on pentane-decane mixture [27]. This comparison has been realized averaging on all our simulation data (that corresponds to around 0.3 μs of a continuous run) to obtain the more reliable estimation of the transport coefficients.

ACKNOWLEDGMENTS

A.P. gratefully acknowledges Elf Exploration Production for financial support. We thank F. Montel for his interest in and support of this work, and J. Petravic for useful discussions on the subject. We thank J. C. Legros as well for clarifications on experimental details. Finally we thank the supercomputing center IDRIS (CNRS) for a generous allocation of time on parallel computer CRAYT3E.

APPENDIX

In this appendix we study the dynamical responses to the impulsive excitation described in Sec. IV A 2, as a function of the imposed field strength.

In Fig. 18 we see the form of the direct response to the mass excitation. The initial value of this response does not change with the field, while the progression in time undergoes important modifications. This means that in the expansion (23),

$$R_{\alpha\beta}(t) = \mathcal{L}_{\alpha\beta}(t) + b_{\alpha\beta}(t)F_e^2 + c_{\alpha\beta}(t)F_e^4 + d_{\alpha\beta}(t)F_e^6,$$

$$\alpha, \beta = 1, Q$$

we have $b_{11}(0)=0, c_{11}(0)=0, d_{11}(0)=0$. This is not the case of the direct response to a heat excitation, shown in Fig. 19. The change arises from the very beginning and already at short times ($\sim 0.3\tau$) one sees a negative peak appearing. We interpret this as the response of the system to a very strong δ-like excitation, i.e., to a perturbation that induces a ''large'' displacement of particles and therefore a transient, induced, negative heat flux. This is not the case for R_{11}, since the interdiffusive flux is just controled by the perturbation, and the thermostat easily removes the produced heat.

As for the cross responses, on Fig. 20 one can see that due to the heat excitation. Again in this case, where we measure a mass flux, we note that in the above expansion, $b_{1Q}(t) = 0, c_{1Q}(t) = 0, d_{1Q}(t) = 0$ at very short times. For low fields we have one first negative peak, a second one is positive and then the correlation function goes to zero from positive values. As the field increases, we note that the first negative peak becomes less deep and that a third negative peak arises. On Fig. 21, we reported the cross response to a mass excitation. The situation is opposed with respect to the other cross response, for the first negative peak, that is the peak becomes deeper as the imposed field increases. We can conclude that the two cross responses, out of the linear region, are very different and hence the Onsager reciprocity relations for these responses are not valid.

[1] D. MacGowan and D.J. Evans, Phys. Rev. A **34**, 2133 (1986); **36**, 948 (1987).
[2] G.V. Paolini and G. Ciccotti, Phys. Rev. A **35**, 5156 (1987).
[3] P. Sindzingre, G. Ciccotti, C. Massobrio, and D. Frenkel, Chem. Phys. Lett. **136**, 35 (1987).
[4] R. Vogelsang, C. Hoheisel, G. Paolini, and G. Ciccotti, Phys. Rev. A **36**, 3964 (1987).
[5] D. Longrée, J. Legros, and G. Thomaes, J. Phys. Chem. **84**, 3480 (1980).
[6] D. Longrée, thèse de doctorat, Université Libre de Bruxelles, 1979.
[7] S. de Groot and P. Mazur, *Non-Equilibrium Thermodynamics* (Dover, New York, 1984).
[8] S. de Groot, Ph.D. thesis, Amsterdam, 1945.
[9] W.W. Wood, J. Stat. Phys. **57**, 675 (1989).
[10] J. Irwing and J. Kirkwood, J. Chem. Phys. **18**, 817 (1950).
[11] D.J. Evans and P.T. Cummings, Mol. Phys. **72**, 893 (1991).
[12] S. Sarman and D.J. Evans, Phys. Rev. A **45**, 2370 (1992).
[13] S. Sarman and D.J. Evans, Phys. Rev. A **46**, 1960 (1992).
[14] R. Zwanzig, J. Chem. Phys. **40**, 2527 (1964).
[15] D.J. Evans, Phys. Lett. A **91A**, 457 (1982).
[16] D.J. Evans and G.P. Morriss, *Statistical Mechanics of Non-equilibrium Liquids* (Academic Press, New York, 1990).
[17] B.L. Holian and D.J. Evans, J. Chem. Phys. **83**, 3560 (1985).
[18] P.J. Daivis and D.J. Evans, Chem. Phys. **198**, 25 (1995).
[19] G. Ciccotti, G. Jacucci, and I.R. McDonald, J. Stat. Phys. **21**, 1 (1979).
[20] G. Ciccotti, C. Pierleoni, and J. Ryckaert, in *Microscopic Simulation of Complex Hydrodynamic Phenomena*, edited by M. Marechal and B. Holian (Plenum Press, New York, 1992).
[21] W.G. Hoover and W.T. Ashurst, in *Theoretical Chemistry: Advances and Perspectives*, edited by H. Eyring and D. Henderson (Academic Press, New York, 1975), Vol. 1, pp. 1–51.
[22] C. Massobrio and G. Ciccotti, Phys. Rev. A **30**, 3191 (1984).
[23] M. Ferrario, G. Ciccotti, B.L. Holian, and J.P. Ryckaert, Phys. Rev. A **44**, 6936 (1991).
[24] A. Tenenbaum, G. Ciccotti, and R. Gallico, Phys. Rev. A **25**, 2778 (1982).
[25] B. Hafskjold and S.K. Ratkje, J. Stat. Phys. **78**, 463 (1995).
[26] J.-P. Ryckaert, A. Bellemans, G. Ciccotti, and G. Paolini, Phys. Rev. A **39**, 259 (1989).
[27] A. Perronace, C. Leppla, F. Leroy, B. Rousseau, and S. Wiegand, J. Chem. Phys. **116**, 3718 (2002).